

NANOPHOTONICS

PACS numbers: 78.67.Bf; 78.67.Sc; 71.35.Aa; 73.20.Mf; 81.07.–b
DOI: 10.1070/QE2015v045n12ABEH015869

Light absorption and plasmon–exciton interaction in three-layer nanorods with a gold core and outer shell composed of molecular J- and H-aggregates of dyes

B.I. Shapiro, E.S. Tyshkunova, A.D. Kondorskiy, V.S. Lebedev

Abstract. **Optical properties of hybrid rod-like nanoparticles, consisting of a gold core, an intermediate passive organic layer (spacer) and outer layer of ordered molecular cyanine dye aggregates, are experimentally and theoretically investigated. It is shown that these dyes can form not only ordered J-aggregates but also H-aggregates (differing by the packing angle of dye molecules in an aggregate and having other spectral characteristics) in the outer shell of the hybrid nanostructure. Absorption spectra of synthesised three-layer nanorods are recorded, and their sizes are determined. The optical properties of the composite nanostructures under study are found to differ significantly, depending on the type of the molecular aggregate formed in the outer shell. The experimental data are quantitatively explained based on computer simulation using the finite-difference time-domain (FDTD) method, and characteristic features of the plasmon–exciton interaction in the systems under study are revealed.**

Keywords: *nanophotonics, hybrid metalorganic nanostructures, localised plasmons, molecular J- and H-aggregates, Frenkel excitons, plasmon–exciton interaction.*

1. Introduction

When solving numerous fundamental and applied problems of photonics, optoelectronics and near-field optics, the analysis of the spectral and nonlinear optical properties of various hybrid nanostructures and their interaction with light is of great importance. Hybrid nanostructures and new composite materials are widely used to design next-generation photonic and optoelectronic devices, such as nanolasers [1–4], solar cells [5–9] and light-emitting diodes [10–13]. Composite materials are applied in metal-coated optical nanowaveguides [14–17] and in hybrid plasmonic waveguides [18, 19]. Nanodevices and hybrid nanostructures of different types are also developed to increase significantly the electric field strength and provide subwavelength field localisation. They include, in particular, tapered metallised near-field optical probes with a dielectric [20–24] or semiconductor [25–28] core and structures designed for fluorescence studies in the visible range [29] and for THz generation in an array of plasmonic nanoparticles [30]. The unique optical properties of various composite nanoparticles and nanostructures of different shapes and sizes are promising for biological and medical applications (see, e.g., [31, 32]).

In recent years, much attention has been paid to investigations and practical developments in the field of organic optoelectronics and nanophotonics (see [33, 34]). Such studies are closely related to the design of hybrid nanostructures and nanomaterials containing both organic and inorganic components. A promising feature of these nanoobjects is the lower cost of organic materials for many applications in comparison with their inorganic analogues. In addition, organic materials are often characterised by unique optical and electrical properties. Currently, various quantum-confinement nanostructures, including colloidal semiconductor quantum dots (see review [35]), nanoplatelets [36, 37] and nanoscrolls [38], are widely used as an inorganic component of hybrid nanostructures and composite materials. These objects are promising for designing optoelectronic and light-emitting devices [39–42] as a base of power-saving and stable light sources for illumination, indication and data imaging.

Another rapidly progressing field of research and development is at the intersection of nanoplasmonics and organic photonics. In particular, the spectral characteristics of various hybrid metalorganic nanostructures (the organic component of which has a form of ordered molecular cyanine dye aggregates) have been intensively investigated. Highly organised aggregates consist of noncovalently bound organic dye molecules; in these aggregates, electronic excitations of individual molecules are collectivised (due to translational order) to form Frenkel excitons [43–45]. These nanostructures have unique optical properties, including a large oscillator strength, ultrashort radiative lifetime and high nonlinear susceptibility. Therefore, they are considered as an organic component in designing next-generation photonic and optoelectronic devices. They are also applied for spectral sensitisation of classical photographic materials based on silver halides [46, 47].

There are two main types of ordered cyanine dye aggregates: J- and H-aggregates [43, 44]. Their structures differ by the packing angle of molecules in the aggregate. The packing angle in H-aggregates exceeds that in J-aggregates [46–48]. The molecular packings in J- and H-aggregates are, respectively, of brickwork and ladder types. The packing angle determines the preferred direction of the aggregate growth: it occurs along the long molecular axis in J-aggregates and along the direction perpendicular to the long axis in H-aggregates. The formation of J- and H-aggregates leads, respectively, to bathochromic and hypsochromic shifts of absorption bands with respect to the molecular band.

B.I. Shapiro, E.S. Tyshkunova M.V. Lomonosov Moscow State University of Fine Chemical Technologies, prosp. Vernadskogo 86, 119571 Moscow, Russia; e-mail: bishapiro@mail.ru, ringing-jump@mail.ru;
A.D. Kondorskiy, V.S. Lebedev P.N. Lebedev Physics Institute, Russian Academy of Sciences, Leninsky prosp. 53, 119991 Moscow, Russia; Moscow Institute of Physics and Technology, Institutskii per. 9, 141700 Dolgoprudnyi, Moscow region, Russia;
e-mail: kondor@sci.lebedev.ru, vlebedev@sci.lebedev.ru

Received 2 June 2015; revision received 18 October 2015
Kvantovaya Elektronika **45** (12) 1153–1160 (2015)
Translated by Yu.P. Sin'kov

Most of the studies in the field of optics and spectroscopy of metalorganic nanostructures and materials were performed for hybrid systems with an organic component in the form of J- rather than H-aggregates of dyes. A number of studies were devoted, in particular, to the interaction of Frenkel excitons (contributing to the J-band of dyes) with surface plasmons in hybrid metalorganic nanostructures having planar geometry (e.g., in thin metal films coated by ordered molecular J-aggregates and in organic semiconductors (cyanine dyes incorporated into a polymer matrix) deposited on a metal film [49–52]). In this case, Frenkel excitons are electromagnetically coupled with plasmons propagating along the planar metal–insulator or metal–semiconductor interface.

There are also many experimental and theoretical investigations of the spectral characteristics of hybrid nanostructures composed of a metal core and an outer shell of ordered molecular J-aggregates of cyanine dyes. They include, in particular, a series of studies of two-layer (see [53–62] and references therein) and three-layer [63–65] spherical metalorganic nanoparticles and composite metalorganic structures in the form of nanorods [66–69]. In these studies, the effects of electromagnetic coupling of molecular excitons with localised plasmons were investigated by an example of systems composed of a gold or silver core and J-aggregates of several different cyanine dyes. Along with this, the results of studying the optical properties of hybrid nanoparticles and nanorods with a metal core, the outer shell of which is formed by ordered molecular H-aggregates [48], are of great interest.

Some cyanine dyes in aqueous solutions are known to form aggregates of both types. For example, it was found recently [70] that such a dye as triethylammonium salt of 3,3′-di(γ-sulfopropyl)-5,5′-dichloro-9-methyl-thiacarbocyanine betaine forms not only H-aggregates but also J-aggregates in a certain concentration range, because these two aggregate forms have similar formation energies. One of these dyes is our object of study: Dye1 [triethylammonium salt of 3,3′-di-(γ-sulfopropyl)-6,6′-dimethoxy-8,10-dimethylene-thiacarbocyanine betaine]; this dye is unique because its H-band lies in the vicinity of $\lambda = 520$ nm, while the J-band is near $\lambda = 725$ nm. The effects of plasmon–exciton interaction in this dye can be investigated using a hybrid system composed of identical gold nanorods with a length of about 50 nm [which exhibit two plasmonic bands, peaking at about 525 and 750 nm, due to two different (transverse and longitudinal) plasmonic modes] as a metal core. Thus, the spectral position of the H-band of the dye under study is close to the peak of the short-wavelength plasmonic band at $\lambda = 525$ nm, and the position of its long-wavelength J-band is close to the peak of the long-wavelength plasmonic band at $\lambda = 750$ nm.

In this paper, we report the results of experimental and theoretical study of the spectral characteristics of three-layer metalorganic nanorods of the Au/TMA/J-aggregate and Au/TMA/H-aggregate types, the outer shell of which is synthesised from a dye capable of forming simultaneously ordered J- and H-aggregates. The organic TMA spacer [N,N,N-trimethyl-(11-mercaptoundecyl)ammonium chloride] in these hybrid structures plays the role of a passive dielectric spacer between the gold core of the system and its outer layer, formed by ordered molecular dye aggregates.

2. Experimental

To fabricate gold nanorods, a nucleation solution was initially prepared by reducing an $HAuCl_4$ aqueous solution with sodium boron hydride according to the technique described in [71]. To this end, 0.6 mL of 0.01 M $NaBH_4$ aqueous solution, previously cooled with ice, were added to 0.65 mL of 0.01 M $HAuCl_4$ aqueous solution, mixed with 17 mL of 0.1 M aqueous solution of surfactant [N-cetyl-N,N,N-trimethyl ammonium bromide (CTAB, Sigma-Aldrich)]. The thus prepared nucleation solution was kept in a thermostat for 2 h at 30 °C. To form rod-like gold nanoparticles, 70 μL of 0.01 M $AgNO_3$ aqueous solution and 64 μL of 0.1 M aqueous solution of L-ascorbic acid were added to 0.4 mL of 0.01 M $HAuCl_4$ aqueous solution mixed with 9.5 mL of 0.1 M CTAB aqueous solution [72–74]. Then 20 μL of nucleation solution were added to this composition. The newly formed mixture was kept without stirring in a thermostat for 3 h at 30 °C to prepare a hydrosol, which was then centrifuged at a speed of 13000 rpm for 20 min, and a precipitate was decanted from the liquid. The $HAuCl_4$ and $AgNO_3$ agents were, respectively, of chemically pure and reagent grades. The cyanine dye [triethylammonium salt of 3,3′-di(γ-sulfopropyl)-6,6′-dimethoxy-8,10-dimethylene-thiacarbocyanine betaine] used to form hybrid metalorganic nanoparticles was synthesised at the Institute of Organic Chemistry, National Academy of Sciences of Ukraine.

To obtain gold nanorods coated by a passive organic TMA [N,N,N-trimethyl-(11-mercaptoundecyl) ammonium chloride] (ProChimia) shell, the precipitate was redispersed in 10 mL of 2×10^{-3} M aqueous solution of TMA, after which the sol was stirred at a moderate speed with a magnetic agitator for 2 h. The TMA excess was removed by decantation of the precipitate from the liquid after hydrosol centrifugation at a speed of 13000 rpm for 20 min. The two-component systems (nanorods composed of a metal gold core and an organic TMA shell) are denoted below as Au/TMA. Their transmission electron microscopy (TEM) images (JEOL JEM-2100 microscope) are shown in Fig. 1a.

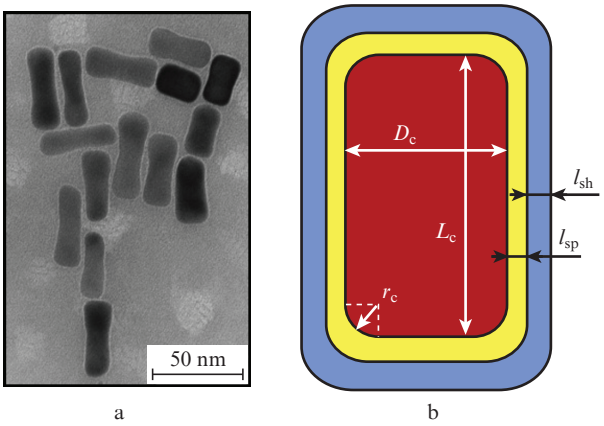

Figure 1. (a) TEM image of two-component Au/TMA nanoparticles and (b) a schematic of the structure of a three-component Au/TMA/Dye nanorod, consisting of a gold core with a longitudinal size L_c, diameter D_c and curvature radius r_c at the rod ends; an outer shell of ordered molecular dye aggregates of thickness l_{sh}; and a passive organic spacer of thickness l_{sp}.

To form three-component Au/TMA/Dye1 nanosystems (consisting of a gold core, a passive organic TMA layer and an outer layer of molecular aggregates), 1 mL of 5×10^{-5} M aqueous solution of cyanine dye Dye1 was added to 4 mL of the hydrosol of two-component rod-like Au/TMA nanopar-

Table 1. Structure and spectral properties of the dyes under study.

Dye	Molecular mass/ g mol^{-1}	Wavelength λ_{max} in C_2H_5OH/nm	Extinction coefficient in C_2H_5OH/L mol^{-1} cm^{-1}
Dye1 [triethylammonium salt of 3,3′-di(γ-sulfopropyl)-6,6′-dimethoxy-8,10-dimethylene-thiacarbocyanine betaine]	740	629	14.2×10^4
Dye2 [triethylammonium salt of 3,3′-di(γ-sulfopropyl)-5-chloro-4′,5′-benzo-thiamonomethinecyanine betaine]	694	445	8.3×10^4
Dye3 [triethylammonium salt of 3,3′-di(γ-sulfopropyl)-4′,5′-[1″,5″-dimethylinda-(3″,2″)]-thiathiazolomonomethinecyanine betaine]	694	466	2.9×10^4

ticles. The spectral characteristics of this dye (and the two other dyes investigated in this study, Dye2 and Dye3) are listed in Table 1, and the structure of the synthesised three-component Au/TMA/Dye1 nanorods is presented in a simplified form in Fig. 1b.

The absorption spectra of aqueous solutions of hybrid nanorods under study (placed in 1-cm-thick glass cells) were recorded on a Beckman spectrophotometer (United States). A bidistillate was used to prepare all aqueous solutions. The absorption spectra of Dye1 in an aqueous solution, rod-like gold particles coated by a passive organic TMA layer, and rod-like gold particles with a passive TMA spacer and adsorbed cyanine dye layer (Au/TMA/Dye1) are shown in Fig. 2. It is noteworthy that the spectrum of the dye in an aqueous solution [curve (*1*)] has three absorption peaks, which are due to a monomer (M) and two dimers (D_1 and D_2). Curve (*2*) in Fig. 2 is the spectrum of two-component Au/TMA particles in an aqueous solution, i.e., the spectrum of plasmonic vibrations of gold nanorods with a thin shell of passive organic TMA layer. This curve has two absorption peaks at λ = 525 and 750 nm, which are due to the existence of two plasmonic modes for gold nanorods: transverse (short-wavelength) and longitudinal (long-wavelength), respectively. Curve (*3*) in Fig. 2 is the absorption spectrum of three-component Au/TMA/Dye1 particles. It can be seen that the absorption spectrum of Au/TMA/Dye1 particles exhibits an absorption dip in the plasmonic band with λ_{max} = 750 nm due to the plasmon–exciton interaction with the dye J-aggregate (minimum at λ = 725 nm). In contrast, the absorption is much higher within the short-wavelength plasmonic band at $\lambda \approx 520-525$ nm.

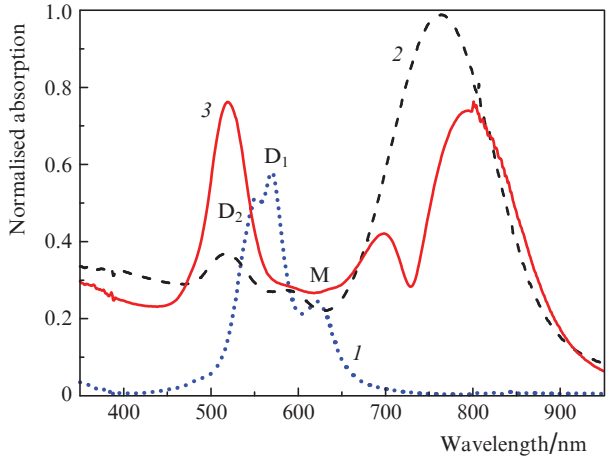

Figure 2. Absorption spectra of (*1*) an aqueous solution of Dye1 at a concentration of 1×10^{-5} M, (*2*) a sol of two-component Au/TMA nanorods and (*3*) a sol of three-component Au/TMA/Dye1 nanorods.

Note that this band is absent in the spectrum of aqueous dye solution [Fig. 2, curve (*1*)]. Thus, it is purely the result of adsorption of Dye1 on gold nanorods coated by a TMA layer.

A reasonable question arises: is the occurrence of a narrow absorption band of the H-aggregate in the vicinity of the short-wavelength ('transverse') plasmonic band a specific feature of this band or is it related to the structure of the molecular dye aggregate? We found that the increase in the photoabsorption of three-component Au/TMA/Dye1 particles in the short-wavelength spectral region is not an exceptional feature of this plasmonic 'transverse' mode. To justify this conclusion, additional spectroscopic measurements were performed on composite metalorganic nanoparticles (Au/TMA/Dye2 and Au/TMA/Dye3) of spherical shape, fabricated using other two cyanine dyes, Dye2 and Dye3 (see Table 1), which have light absorption maxima near the peak of the plasmonic mode of spherical gold nanoparticles (λ_{max} = 520 nm). These dyes were synthesised at the State Research and Design Institute of Chemical and Photographic Industry (Gosniikhimfotoproekt) (Moscow).

Spherical gold nanoparticles (cores of hybrid Au/TMA/Dye2 and Au/TMA/Dye3 nanoparticles) were obtained according to the technique described in [75]. Specifically, a mixture of 50 mg of $HAuCl_4\cdot3H_2O$, 1.0 g (1.2 mL) of oleylamine, and 1 mL of toluene was added (without stirring) to a solution of 1.7 g (2.9 mL) of oleylamine in 49 mL of toluene, boiling at 140 °C. After adding hydrochloroauric acid with oleylamine in toluene, the solution colour gradually changed to intense red for several minutes, which indicated the formation of gold nanoparticles. The colloidal solution was boiled for two hours, after which the suspension of gold nanoparticles coated by oleylamine was cooled to room temperature. Then 25 mL of methanol were added to 10 mL of the suspension obtained to precipitate the product. The particles were separated from the oleylamine excess using 15-min centrifugation at a speed of 6500 rpm. The precipitate was redispersed in 15 mL of toluene, after which 1 mL of TMA solution in methanol (30 mM) was added. Then the mixture was centrifuged for 10 min at a speed of 6000 rpm. The thus obtained precipitate was washed thrice with ethyl acetate. Finally, the dried solid precipitate (Au/TMA) was redispersed in double-distilled water to an optical density of about 0.4 at 350 nm (in a 1-cm cell). To form J-aggregates on the surface of gold nanoparticles coated by a TMA layer, one volume of an aqueous solution of Dye2 with a concentration of 5×10^{-5} M was added to four volumes of hydrosol of Au/TMA nanoparticles.

The photoabsorption spectra of synthesised spherical Au/TMA/Dye2 nanoparticles revealed a dip near the plasmonic band (at λ = 488 nm) (Fig. 3). This situation is typical of strong electromagnetic coupling of a plasmon in the core of a spherical metalorganic nanoparticle with a Frenkel exciton

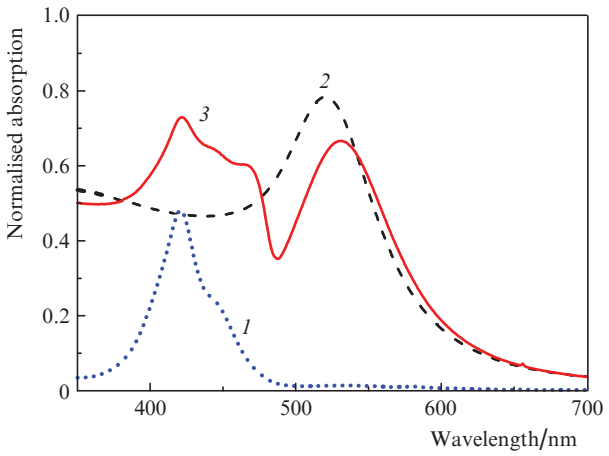

Figure 3. Absorption spectra of (*1*) an aqueous solution of Dye2 at a concentration of 2×10^{-5} M, (*2*) a sol of two-component Au/TMA nanospheres and (*3*) a sol of three-component Au/TMA/Dye2 nanospheres.

localised in the outer J-aggregate shell. Our studies showed that Dye3 behaves similarly when used to form an outer organic layer of molecular J-aggregates in hybrid spherical Au/TMA/Dye3 nanoparticles. In this case, the photoabsorption spectrum of these three-component nanoparticles also exhibits a characteristic dip at λ = 512 nm, which lies in the vicinity of the plasmonic band of gold nanoparticles and the absorption band of molecular J-aggregate (see Fig. 4).

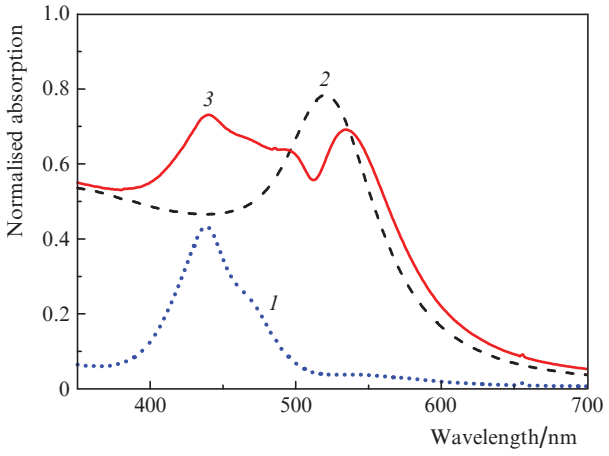

Figure 4. Absorption spectra of (*1*) an aqueous solution of Dye3 at a concentration of 2×10^{-5} M, (*2*) a sol of two-component Au/TMA nanospheres and (*3*) a sol of three-component Au/TMA/Dye3 nanospheres.

Thus, a comparison of the results presented in Figs 2–4 shows definitely that the plasmon–exciton interaction caused by electromagnetic coupling of dye J-aggregates with the gold core of metalorganic nanosystems of different shapes similarly manifests itself in the spectral regions near the short-wavelength (for nanospheres) and long-wavelength (for nanorods) plasmonic bands and is accompanied by a photoabsorption dip in these bands. Therefore, in the case under consideration, the character and specificity of the interaction of plasmons with Frenkel excitons of dye aggregates is undoubtedly related to the specificity of organic ordered nanostructures (molecular J- or H-aggregates) rather than to the plasmonic mode type.

In this context, we should recall that, according to the modern concepts, J- and H-aggregates of cyanine dyes are formed from dimers via the 'block' mechanism (see, e.g., [45, 76]), which is shown in a simplified form in Fig. 5. The difference between J- and H-aggregates is in the type of molecular packing: the former are characterised by brickwork packing (Fig. 5a), whereas the packing of the latter is of ladder type (Fig. 5b).

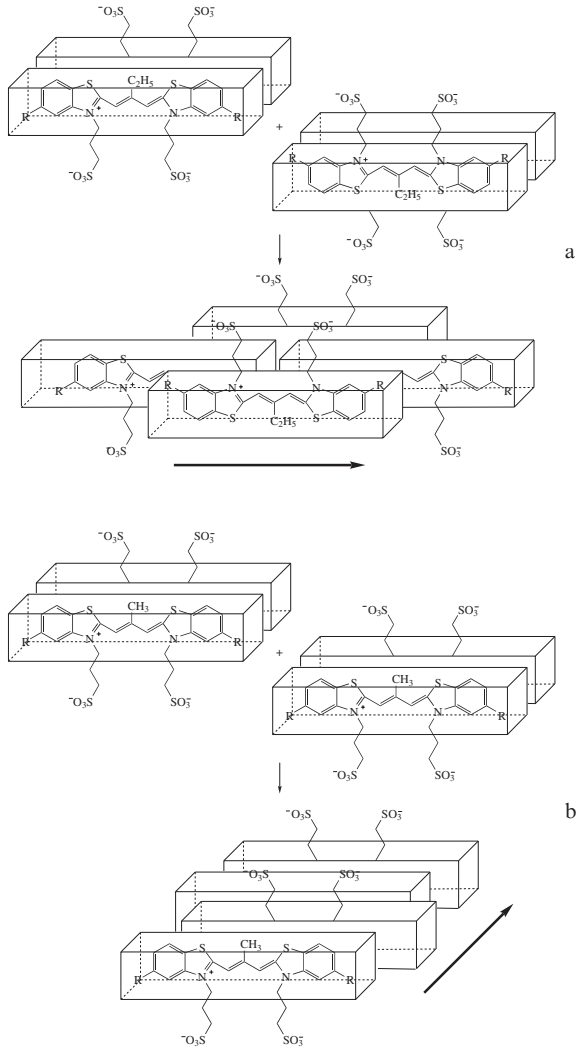

Figure 5. Schematic diagram of the formation of ordered molecular (a) J- and (b) H-aggregates of cyanine dyes. Dark arrows indicate the aggregate growth direction.

3. Mathematical simulation and comparison of theory with experiment

To analyse and explain the experimental spectral data, we performed mathematical simulation of the absorption spectra of nanostructures under study. The resulting absorption spectra recorded in a colloidal solution were considered as the sum

$$\sigma(\omega) = \sum_j c_j \sigma_j(\omega), \quad (1)$$

where $\sigma_j(\omega)$ are the absorption cross sections of individual components of the solution and c_j are their weighting factors, proportional to their concentrations.

When carrying out numerical simulation of the absorption spectra of synthesised nanorods, the Maxwell equations were solved using the finite-difference time-domain (FDTD) method [77]. A computer program making it possible to calculate absorption cross sections with allowance for the contributions of all multipoles was developed based on the library with an open initial code MEEP [78, 79].

The optical properties of the materials composing the nanostructures under study are determined by their permittivities. Our calculations were based on the standard representation:

$$\varepsilon(\omega) = \varepsilon_\infty + \sum_{n=1}^{N} \frac{f_n \omega_n^2}{\omega_n^2 - \omega^2 - i\omega\gamma_n}, \quad (2)$$

where ε_∞ is the permittivity at a frequency $\omega \to \infty$ and ω_n, γ_n and f_n are, respectively, the frequency, width and amplitude of the nth ($n = 1, ..., N$) resonance.

The parameters of function (2) (describing permittivity) for gold, with allowance for the contributions of free and bound electrons and the size effect caused by electron scattering at the interface between the gold rod and passive organic layer, were chosen as follows. Initially, the parameters in (2) were chosen so as to fit in the best way the experimental data on the real and imaginary parts of permittivity that were obtained in [80]. Then these parameters were corrected to describe the experimental data of [55] for the light absorption cross section of a two-layer Au/TMA nanosphere, with a core diameter of 16 nm. Since all experiments with hybrid metal-organic nanostructures were performed in aqueous solutions, we used a value of 1.78 for permittivity ε_h of the environment (solvent) in the visible spectral range.

The permittivity parameters for the materials under study, found from calculations, are listed in Table 2.

Table 2. Parameters of function (2) for the materials composing a three-component metalorganic Au/TMA/Dye1 nanorod.

Material	ε_∞	ω_n/eV	γ_n/eV	f_n
Gold	3.795	$\omega_1 \approx 0$	0.174	$72.56/\omega_1^2$
		0.309	0.0136	14.76
		0.468	0.0207	2.118
		1.198	0.525	0.9847
		3.431	0.851	0.7029
		2.674	0.554	0.3370
		2.956	0.681	0.5667
		4.08	1.160	1.392
TMA	2.19	0	0	0
J-aggregate	2	1.710	0.0130	0.0484
H-aggregate	2	2.291	0.128	0.455

The shape of the nanostructures studied is shown in Fig. 1a. Their geometric parameters were determined from TEM data. The average diameter D_c of the gold cores of nanorods was 14 nm, and the curvature radius was $r_c = 2$ nm. The spread of nanorod lengths leads to an inhomogeneous broadening in the long-wavelength spectral region (Fig. 6). To describe this broadening, we calculated the absorption cross sections for nanorods with different gold core lengths. The contributions of the cross sections found for different-length nanorods were taken into account as individual terms in formula (1). Thus, we found the length distributions of metal cores (see Fig. 7). The ratio of the number of nanostructures with the H-aggregate shell to the number of nanostructures with the J-aggregate shell is 7 : 10.

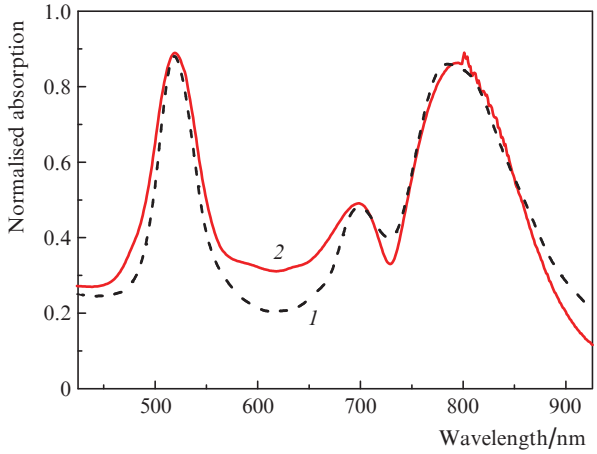

Figure 6. (*1*) Simulated light absorption spectrum of a solution of Au/TMA/Dye1 nanorods and (*2*) experimental data.

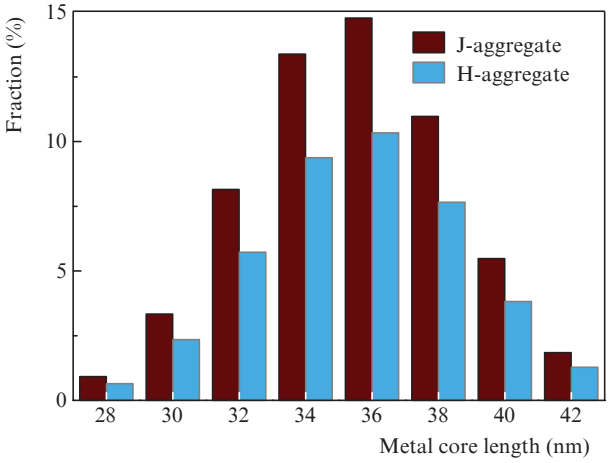

Figure 7. Length histogram for metal cores of Au/TMA/Dye1 nanorods with J- and H-aggregate shells.

The thickness of the passive spacer was found (based on TEM data) to be $l_{sp} = 1$ nm. The thicknesses of the outer layers, l_J and l_H for J- and H-aggregates, respectively, were obtained in the same way as the parameters of the function describing the permittivity of these materials, i.e., by their fitting to describe in the best way the experimental data on light absorption spectra. For the hybrid nanorods with outer shells composed of J- and H-aggregates, these parameters were determined to be $l_J = 5$ nm and $l_H = 8$ nm. These thicknesses of the outer molecular-aggregate shell are in agreement with the values reported in a number of studies on the struc-

ture and spectral properties of hybrid nanoparticles with a metal core and outer aggregate layer of cyanine dyes (see, e.g., [81–83]).

It is noteworthy that simultaneous fitting of the layer thicknesses and most of the parameters of the permittivity function based on only spectroscopic data does not lead to any significant ambiguity in determining parameters, because, due to the effects of strong plasmon–exciton coupling, the influence of different parameters, being qualitatively different, determines the general behaviour, number and specific wavelengths of the spectral features observed. In particular, we showed that, as a result of variation in the reduced transition oscillator strength in both J- and H-bands of a dye, with other aggregate parameters [centre of the absorption band, its width, and ε_∞; see (2)] kept the same, the resonance amplitude affects significantly the resulting character of the absorption spectrum. In addition, the real part of permittivity (in particular, constant ε_∞) only slightly affects the character of the absorption spectrum of dye solutions; however, it determines to a great extent the photoabsorption spectra of composite metal-organic nanostructures. Analysis of the calculation results suggests that a relatively small variation in the physical parameters of the nanosystems under study changes significantly the character of their spectra.

We compared the results of simulation of the absorption spectrum of a solution of three-component Au/TMA/Dye1 nanorods with the experimental dependence of the absorptive ability of nanorod solution on light wavelength λ (see Fig. 6). The simulation of the optical properties of hybrid metalorganic nanorods by the FDTD method yielded good agreement between the theory and experiment.

4. Conclusions

The most important results of the work are as follows:

(1) We have investigated the optical properties of a cyanine dye capable of forming simultaneously monomers M, dimers D_1 and D_2, and ordered molecular aggregates of J- and H-types on the surface of gold nanoparticles coated by a thin passive TMA organic layer. A technique of forming rod-like hybrid nanoparticles, Au/TMA/J-aggregate and Au/TMA/H-aggregate, with the aid of this dye has been developed. The geometric parameters of synthesised hybrid nanorods are determined and their spectroscopic properties are investigated.

(2) Characteristic differences in the optical properties of hybrid Au/TMA/J-aggregate and Au/TMA/H-aggregate nanostructures are experimentally found for the dye under study (Fig. 2). The absorption spectrum of Au/TMA/Dye1 nanorods exhibits a dip in the vicinity of $\lambda \approx 725$ nm, which is due to the strong electromagnetic coupling between a Frenkel exciton of the J-aggregate of the dye and a longitudinal plasmon of the nanorod. In contrast, the absorption intensity increases in the region of the short-wavelength range at $\lambda \approx 520–525$ nm, which is due to transverse plasmons in nanorods.

(3) Significant qualitative and quantitative differences in the behaviour of the absorption spectra of rod-like metal-organic nanoparticles and the spectra of hybrid two-layer and three-layer spherical particles, which have been investigated previously in detail [56–65], are demonstrated.

(4) A computer simulation of the absorption spectra of rod-like metalorganic Au/TMA/J-aggregate and Au/TMA/H-aggregate nanoparticles has been performed using the FDTD method. The calculation results are compared with the experimental data. The experimental data of this study are explained, and their reliable quantitative description is presented.

(5) As a result of simulation of the absorption spectra, the parameters of the functions describing the permittivity have been obtained based on existing experimental data. These parameters determine the optical properties of J- and H-aggregates of the dye under study. We have also found the parameters of the function describing the permittivity of rod-like gold particles. These parameters take into account the contributions of free and bound electrons and the size effect caused by the electron scattering at the interface between the metal and organic TMA spacer.

(6) The data on the optical properties of rod-like metal-organic nanostructures are of direct practical interest for rapidly developing fundamental and applied research in the field of organic and hybrid organic and inorganic optoelectronics and nanophotonics.

Acknowledgements. This work was supported by the Russian Science Foundation (Project No. 14-22-00273). We are grateful to Yu.L. Slominskii and A.I. Tolmachev (Institute of Organic Chemistry, National Academy of Sciences of Ukraine) for supplying cyanine Dye1 and to T.G. Zemlyanova (Gosniikhimfotoproekt, Moscow) for supplying cyanine Dye2 and Dye3 (see Table 1).

References

1. Ma R., Oulton R.F., Sorger V.J., Zhang X. *Laser Photon. Rev.*, **7**, 1 (2012).
2. Röder R., Wille M., Geburt S., Rensberg J., Zhang M., Lu J.G., Capasso F., Buschlinger R., Peschel U., Ronning C. *Nano Lett.*, **13**, 3602 (2013).
3. Liu X., Zhang Q., Yip J.N., Xiong Q., Sum T.C. *Nano Lett.*, **13**, 5336 (2013).
4. Khurgin J.B., Sun G. *Nat. Photonics*, **8**, 468 (2014).
5. Skompska M. *Synthetic Metals*, **160**, 1 (2010).
6. Reiss P., Couderc E., De Girolamo J., Pron A. *Nanoscale*, **3**, 446 (2011).
7. Lunt R.R., Osedach T.P., Brown P.R., Rowehl J.A., Bulović V. *Adv. Mater.*, **23**, 5712 (2011).
8. Guo C., Lin Y.-H., Witman M.D., Smith K.A., Wang C., Hexemer A., Strzalka J., Gomez E.D., Verduzco R. *Nano Lett.*, **13**, 2957 (2013).
9. Chang L.-Y., Lunt R.R., Brown P.R., Bulović V., Bawendi M.G. *Nano Lett.*, **13**, 994 (2013).
10. Shirasaki Y., Supran G.J., Bawendi M.G., Bulović V. *Nat. Photonics*, **7**, 13 (2013).
11. Vitukhnovskii A.G., Vashchenko A.A., Lebedev V.S., Vasiliev R.B., Brunkov P.N., Bychkovskii D.N. *Fiz. Tekh. Poluprovodn.*, **47**, 962 (2013) [*Semicond.*, **47**, 971 (2013)].
12. I-Ann Lei, Dai-Fu Lai, Trong-Ming Don, Wen-Chang Chen, Yang-Yen Yu, Wen-Yen Chiu. *Mater. Chem. Phys.*, **144**, 41 (2014).
13. Vitukhnovsky A.G., Lebedev V.S., Selyukov A.S., Vashchenko A.A., Vasiliev R.B., Sokolikova M.S. *Chem. Phys. Lett.*, **619**, 185 (2015).
14. Kuznetsova T.I., Lebedev V.S. *Kvantovaya Elektron.*, **32**, 727 (2002) [*Quantum Electron.*, **32**, 727 (2002)].
15. Jones R., Rong H., Liu A., Fang A.W., Hak D., Cohen O. *Opt. Express*, **13**, 519 (2005).
16. Kuznetsova T.I., Lebedev V.S. *Phys. Rev. E*, **78**, 016607 (2008).

17. Gramotnev D.K., Bozhevolnyi S.I. *Nat. Photonics*, **8**, 13 (2014).
18. Chen Z.-X., Wu Z.-J., Ming Y., Zhang X.-J., Lu Y.-Q. *AIP Adv*., **4**, 017103 (2014).
19. Wei W., Zhang X., Ren X. *Nanoscale Res. Lett*., **9**, 599 (2014).
20. Naber A., Molenda D., Fischer U.C., Maas H.-J., Höppener C., Lu N., Fuchs H. *Phys. Rev. Lett*., **89**, 210801 (2002).
21. Kuznetsova T.I., Lebedev V.S. *Kvantovaya Elektron*., **33**, 931 (2003) [*Quantum Electron*., **33**, 931 (2003)].
22. Kuznetsova T.I., Lebedev V.S., Tsvelik A.M. *J. Opt. A: Pure Appl. Opt.*, **6**, 338 (2004).
23. Novotny L., Stranick S.J. *Ann. Rev. Phys. Chem.*, **57**, 303 (2006).
24. Huber C., Trügler A., Hoheneste U., Priorc Y., Kautek W. *Phys. Chem. Chem. Phys*., **16**, 2289 (2014).
25. Yatsui T., Isumi K., Kourogi M., Ohtsu M. *Appl. Phys. Lett*., **80**, 2257 (2002).
26. Kuznetsova T.I., Lebedev V.S. *Pis'ma Zh. Eksp. Teor. Fiz.*, **79**, 70 (2004) [*JETP Lett*., **79**, 62 (2004)].
27. Kuznetsova T.I., Lebedev V.S. *Phys. Rev. B*, **70**, 035107 (2004).
28. Kuznetsova T.I., Lebedev V.S. *Kvantovaya Elektron*., **34**, 361 (2004) [*Quantum Electron*., **34**, 361 (2004)].
29. Kravets V.G., Zoriniants G., Burrows C.P., Schedin F., Geim A.K., Barnes W.L., Grigorenko A.N. *Nano Lett*., **10**, 874 (2010).
30. Polyushkin D.K., Hendry E., Stone E.K., Barnes W.L. *Nano Lett*., **11**, 4718 (2011).
31. Khlebtsov B.N., Liu Z., Ye J., Khlebtsov N.G. *J. Quant. Spectrosc. Radiat. Transfer*, **167**, 64 (2015).
32. Chen K., Lin C.C., Vela J., Fang N. *Anal. Chem*., **87**, 4096 (2015).
33. Agranovich V.M., Gartstein Yu.N., Litinskaya M. *Chem. Rev*., **111**, 5179 (2011).
34. Vitukhnovsky A.G. *Usp. Fiz. Nauk*, **183**, 653 (2013) [*Phys. Usp*., **56**, 623 (2013)].
35. Vasil'ev R.B., Dirin D.N., Gas'kov A.M. *Usp. Khim.*, **80**, 1190 (2011).
36. Mahler B., Nadal B., Bouet C., Patriache G., Dubertret B. *J. Am. Chem. Soc*., **134**, 18591 (2012).
37. Vashchenko A.A., Vitukhnovskii A.G., Lebedev V.S., Selyukov A.S., Vasiliev R.B., Sokolikova M.S. *Pis'ma Zh. Eksp. Teor. Fiz*., **100**, 94 (2014)) [*JETP Lett*., **100**, 86 (2014)].
38. Vasiliev R.B., Sokolikova M.S., Vitukhnovskii A.G., Ambrozevich C.A., Selyukov A.S, Lebedev V.S. *Kvantovaya Elektron*., **45**, 853 (2015) [*Quantum Electron*., **45**, 853 (2015)].
39. Anikeeva P.O., Madigan C.F., Halpert J.E., Bawendi M.G., Bulović V. *Phys. Rev. B*, **78**, 085434 (2008).
40. Vashchenko A.A., Lebedev V.S., Vitukhnovskii A.G., Vasiliev R.B., Samatov I.G. *Pis'ma Zh. Eksp. Teor. Fiz*., **96**, 118 (2012) [*JETP Lett*., **96**, 113 (2012)].
41. Chen Z., Nadal B., Mahler B., Aubin H., Dubertret B. *Adv. Funct. Mater*., **24**, 295 (2014).
42. Selyukov A.S., Vitukhnovskii A.G., Lebedev V.S., Vashchenko A.A., Vasiliev R.B., Sokolikova M.S. *Zh. Eksp. Teor. Fiz.*, **147**, 687 (2015) [*JETP*, **120**, 595 (2015)].
43. Kobayashi T. (Ed.) *J-Aggregates* (Singapore: World Scientific, 1996).
44. Shapiro B.I. *Usp. Khim.*, **75**, 484 (2006).
45. Shapiro B.I. *Ross. Nanotekhnol.*, **3**, 72 (2008).
46. James T.H. *The Theory of the Photographic Process* (New York: Macmillan, 1977).
47. Shapiro B.I. *Teoreticheskie nachala fotograficheskogo protsessa* (Theoretical Fundamentals of Photographic Process) (Moscow: Editorial URSS, 2000).
48. Shapiro B.I., Sokolova L.S, Kuz'min V.A., Tolmachev A.I., Slominskii Yu.L., Briks Yu.L. *Ross. Nanotekhnol*., **7**, 28 (2012).
49. Bellessa J., Bonnand C., Plenet J.C. *Phys. Rev. Lett*., **93**, 036404 (2004).
50. Bonnand C., Bellessa J., Plenet J.C. *J. Non-Cryst. Solids*, **352**, 1683 (2006).
51. Symonds C., Bonnand C., Plenet J.C., Bréhier A., Parashkov R., Lauret J.S., Deleporte E., Bellessa J. *New J. Phys.*, **10**, 065017 (2008).
52. Cade N.I., Ritman-Meer T., Richards D. *Phys. Rev. B*, **79**, 241404 (2009).
53. Wiederrecht G.P., Wurtz G.A., Bouhelier A. *Chem. Phys. Lett.*, **461**, 171 (2008).
54. Lebedev V.S., Vitukhnovsky A.G., Yoshida A., Kometani N., Yonezawa Y. *Colloids Surf. A: Physicochem. Eng. Aspects*, **326**, 204 (2008).
55. Yoshida A., Yonezawa Y., Kometani N. *Langmuir*, **25**, 6683 (2009).
56. Lebedev V.S., Medvedev A.S, Vasil'ev D.N., Chubich D.A., Vitukhnovsky A.G. *Kvantovaya Elektron*., **40**, 246 (2010) [*Quantum Electron*., **40**, 246 (2010)].
57. Lekeufack D.D., Brioude A., Coleman A.W., Miele P., Bellessa J., Zeng L.D., Stadelmann P. *Appl. Phys. Lett*., **96**, 253107 (2010).
58. Lebedev V.S., Medvedev A.S. *Kvantovaya Elektron*., **42**, 701 (2012) [*Quantum Electron*., **42**, 701 (2012)].
59. Vujačić A., Vasić V., Dramićanin M., Sovili S.P., Bibić N., Hranisavljevic J., Wiederecht G.P. *J. Phys. Chem. C*, **116**, 4655 (2012).
60. Lebedev V.S., Medvedev A.S. *J. Russ. Laser Res*., **34**, 303 (2013).
61. Zengin G., Johansson G., Johansson P., Antosiewicz T.J., Käll M., Shegai T. *Scientific Reports*, **3**, 3074 (2013).
62. Antosiewicz T.J., Apell S.P., Shegai T. *ACS Photonics*, **1**, 454 (2014).
63. Yoshida A., Kometani N. *J. Phys. Chem. C*, **114**, 2867 (2010).
64. Medvedev A.S., Lebedev V.S. *Kratk. Soobshch. Fiz. FIAN*, (6), 23 (2010) [*Bulletin of the Lebedev Physics Institute*, **37**, 177 (2010)].
65. Lebedev V.S., Medvedev A.S. *Kvantovaya Elektron*., **43**, 1065 (2013) [*Quantum Electron*., **43**, 1065 (2013)].
66. Wurtz G.A., Evans P.R., Hendren W., Atkinson R., Dickson W., Pollard R.J., Zayats A.V., Harrison W., Bower C. *Nano Lett.*, **7**, 1297 (2007).
67. Yoshida A., Uchida N., Kometani N. *Langmuir*, **25**, 11802 (2009).
68. Shapiro B.I., Kol'tsova E.S., Vitukhnovskii A.G., Chubich D.A., Tolmachev A.I., Slominskii Yu.L. *Ross. Nanotekhnol*., **6**, 83 (2011).
69. Kondorskiy A.D., Kislov K.S., Lam N.T., Lebedev V.S. *J. Rus. Laser Res.*, **36**, 175 (2015).
70. Nekrasov A.D., Shapiro B.I., Kuz'min V.A. *Khim. Vys. Energ.*, **48**, 109 (2014).
71. Sau T.K., Murphy C.J. *Langmuir*, **20**, 6414 (2004).
72. Murphy C.J., Sau T.K., Gole A.M., Orendorff C.J., Gao J., Gou L., Hunyadi S.E., Li T. *J. Phys. Chem. B*, **109**, 13857 (2005).
73. Nikoobakht B., El-Sayed M.A. *Chem. Mater.*, **15**, 1957 (2003).
74. Nishioka K., Niidome Y., Yamada S. *Langmuir*, **23**, 10353 (2007).
75. Misawa K., Ono H., Kobayashi T. *Appl. Phys. Lett*., **63**, 577 (1993).
76. Avakyan A.G., Shapiro B.I., Alfimov M.V. *Dyes Pigm.*, **109**, 21 (2014).
77. Taflove A., Hagness S.C. *Computational Electrodynamics: The Finite-Difference Time-Domain Method* (Norwood: Artech House, 2005).

78. Oskooi A.F., Roundy D., Ibanescu M., Bermel P., Joannopoulos J.D., Johnson S.G. *Comp. Phys. Comm.*, **181**, 687 (2010).
79. http://ab-initio.mit.edu/wiki/index.php/Meep.
80. Johnson P.B., Christy R.W. *Phys. Rev. B*, **6**, 470 (1972).
81. DeLacy B.G., Miller O.D., Hsu C.W., Zander Z., Lacey S., Yagloski R., Fountain A.W., Valdes E., Anquillare E., Soljačić M., Johnson S.G., Joannopoulos J.D. *Nano Lett.*, **15**, 2588 (2015).
82. Gülen D. *J. Phys. Chem. C*, **114**, 13825 (2010).
83. Chen H., Shao L., Woo K.C., Wang J., Lin H.-Q. *J. Phys. Chem. C*, **116**, 14088 (2012).